Phase Transitions Induced by Nanoconfinement in Liquid Water

Nicolas Giovambattista,[1,2] Peter J. Rossky,[3] and Pablo G. Debenedetti[2]

[1]*Department of Physics, Brooklyn College of the City University of New York, Brooklyn, New York 11210 USA*
[2]*Department of Chemical Engineering, Princeton University, Princeton, New Jersey 08544-5263 USA*
[3]*Department of Chemistry and Biochemistry and Institute for Computational Engineering and Sciences, University of Texas at Austin,
Austin, Texas 78712 USA*

We present results from molecular dynamics simulations of water confined by two parallel atomically detailed hydrophobic walls. Simulations are performed at $T = 300$ K and wall-wall separation $d = 0.6$–1.6 nm. At $0.7 \leq d \leq 0.9$ nm, a first order transition occurs between a bilayer liquid (BL) and a trilayer heterogeneous fluid (THF) as water density increases. The THF is characterized by a liquid (central) layer and two crystal-like layers next to the walls. The BL-THF transition involves freezing of the two surface layers in contact with the walls. At $d = 0.6$ nm, the THF transforms into a bilayer ice (BI) upon decompression. Both the BL-THF and BI-THF transitions are induced by the surface regular atomic-scale structure.

The structure and properties of water in nanometer-scale confinement are important in numerous applications and scientific fields. Examples include biological self-assembly, where water mediates the interaction between chemically, electrically, and geometrically complex surfaces [1], fuel cell technology, where rates of proton transport are controlled by membrane hydration [2], nanotribology, where water can control friction between solid surfaces [3], and lab-on-a-chip applications, where water flow in confined geometries occurs under the influence of thermal, mechanical, electrical or substrate chemical patterning driving forces [4]. In such situations, the influence of the confining surface's geometry and chemistry on water's microscopic structure, dynamics and thermodynamics can be profound.

Water's distinctive physical properties include complex phase behavior, which continues to be the subject of intense research activity. Notable aspects include the large number of ice phases [5], and the metastable phase behavior of supercooled water, including the possible existence of one or more phase transitions between distinct forms of deeply supercooled water [6]. A systematic understanding of the influence of confinement on this rich phase behavior is currently lacking.

Although several computational studies have addressed the equilibrium between water vapor and adsorbed phases (e.g., [7–10]), the equilibrium behavior of nanoscopically confined condensed phases has been the subject of comparatively few studies, and most of these have addressed the effect of smooth, structureless walls [11–20]. The freezing of water in carbon nanotubes has been studied by Zeng and collaborators [21,22]. Zangi and Mark investigated freezing under confinement by atomically detailed walls with dispersive, nondirectional interactions [23]. These works have shown the importance of substrate geometry on freezing.

Building upon our recent computational investigations of hydration behavior under nanoscale confinement by atomically detailed nanoscale plates [24,25], here we report two novel phase transitions, which, unlike a homogeneous solid-liquid transition, involve frozen ordered layers templated by the walls: a trilayer heterogeneous fluid (two crystalline layers and a middle fluid layer)-bilayer ice (THF-BI) and a trilayer heterogeneous fluid-bilayer liquid (THF-BL) phase transition.

We perform molecular dynamics (MD) simulations of water confined between infinite parallel walls. Simulations are performed at constant number of molecules, volume, and temperature ($N - V - T$ ensemble). We consider a cubic box of side length $L = 13.86$ nm where two walls are located parallel to the (x, y) plane, equidistant from $z = 0$; the wall area in the primary cell is $A = L \times L = 192.10$ nm^2. Water molecules are located only between the walls and periodic boundary conditions are applied along the unbounded directions x and y. The temperature is fixed at $T = 300$ K; N and the wall-wall distance vary, depending on the simulated density.

We use the silica-based hydrophobic walls implemented in Refs. [24,25]. Briefly, each wall is composed of four layers of SiO$_2$ reproducing the (1, 1, 1) octahedral face of cristobalite [26] (each wall is composed of 3136 atoms). Wall atoms have no charge, only Lennard-Jones potential interactions exist between wall atoms and water oxygen atoms (the interaction parameters are given in Table I of Ref. [24]). The distance between the walls, d, is defined as in Ref. [24] and the confined volume is defined as $V = L^2 \times d$, the density being $\rho = Nm_w/V$ where m_w is the mass of a water molecule. Water molecules are modeled with the extended simple-point-charge (SPC/E) pair potential [27]. Long range interactions are treated using the Ewald sum technique [28,29].

050603-1

Total simulation times range between 300 ps and 2 ns depending on density and wall-wall separation. However, thermodynamic quantities such as pressure become constant after approximately 50–100 ps. Simulations are run for approximately twice the time needed for the system to reach the diffusive regime. In the diffusive regime, the mean square-displacement parallel to the walls increases linearly with time. Only the second half of the simulation is used for data acquisition. We calculate both the pressure perpendicular ($P_\perp$) and parallel ($P_\parallel$) to the walls. $P_\perp$ is obtained as the total force exerted by water molecules on each wall, divided by the wall area. $P_\parallel$ is obtained from the virial expression using the projection of the atom position vectors and forces on the plane parallel to the walls (analogous to the virial expression obtained in Ref. [29] for a bulk system).

For a liquid confined by parallel *immobile* walls, a necessary and sufficient criterion of stability is that $(\partial P_\parallel / \partial \rho)_{d,T,A} > 0$ [30,31]. Figure 1(a) shows $P_\parallel$ as a function of ρ at $d \geq 0.8$ nm. For large separations, $d \geq 1.0$ nm, $P_\parallel(\rho)$ shows a positive slope for $\rho \geq 0.7$ g/cm³, indicating that the system is a single phase. At these conditions, the system is in the liquid phase. At $\rho < 0.7$ g/cm³, bubble formation occurs indicating the coexistence of vapor and liquid phases. Accordingly, $(\partial P_\parallel / \partial \rho)_{d,T,A} < 0$. As $d \to 0.8$ nm, the minimum in $P_\parallel(\rho)$ remains at $\rho = 0.7$ g/cm³. However, a new feature develops in $P_\parallel(\rho)$ as $d \to 0.8$ nm. Specifically, $P_\parallel(\rho)$ shows a finite size loop [32] in the range $\rho \approx 0.85$–1.1 g/cm³ indicating the presence of a first order phase transition. Two phases are observed, a BL at 0.7 g/cm³ $< \rho < 0.9$ g/cm³, and a THF at $\rho \geq 1.05$ g/cm³. The THF is characterized by a central liquid layer and two crystal-like layers next to the walls (see discussion below). We use the terminology *finite size loop* [32], noting also that in our case both finite size and confinement effects are important.

Figure 1(b) shows $P_\parallel(\rho)$ for $d \leq 0.8$ nm. At $d = 0.7$ nm, the loop is barely visible and it disappears as d decreases. At $d = 0.6$ nm, a THF is observed at densities $\rho \geq 1.2$ g/cm³. As the density decreases from 1.2 g/cm³ down to 0.93 g/cm³ [black arrow in Fig. 1(b)], a crystallization into a BI starts to occur at $\rho \approx 1.1$ g/cm³ and patches of BI coexist with liquid patches at $0.93 < \rho < 1.1$ g/cm³. The minimum observed at $\rho \approx 0.93$ g/cm³ corresponds to the point at which a perfect BI is formed. At smaller densities, the crystal sublimes. The same BI was observed in our previous work [24] under different conditions. Recently, the crystallization of nanoconfined water at room temperature has been confirmed [33].

Figure 2(a) shows both $P_\parallel(\rho)$ (from Fig. 1) and $P_\perp(\rho)$ at $d = 0.8$ nm. Only $P_\parallel(\rho)$ shows a loop, while $(\partial P_\perp / \partial \rho)_{d,T,A} \geq 0$. Figure 2(b) shows the density profile, $\rho(z)$ at four densities, above ($\rho = 1.15$, 1.05 g/cm³) and below ($\rho = 0.80$ g/cm³) the first order transition, and at a state in the transition region ($\rho = 0.95$ g/cm³). $\rho(z)$ is the
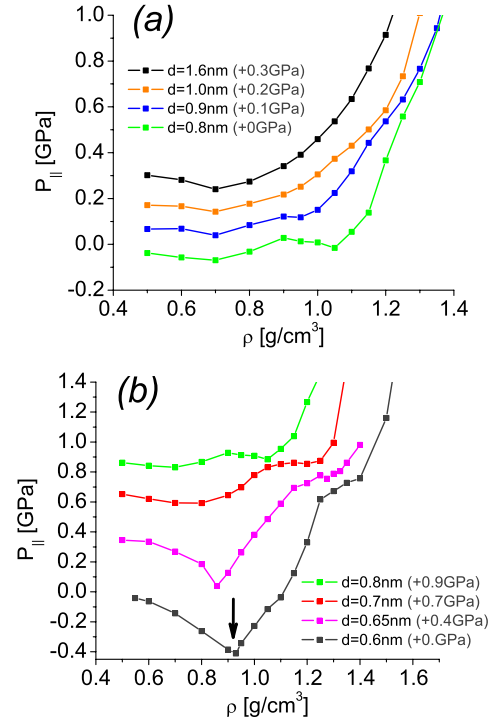

FIG. 1 (color online). Pressure parallel to the walls ($P_\parallel$) as a function of density (ρ), at different wall-wall separations (d); (a) $d \geq 0.8$ nm, (b) $d \leq 0.8$ nm. Error bars are of the order of the symbol size. Curves for a given value of d are shifted in pressure for clarity (shifts are indicated in the labels by pressure values in parenthesis). A finite size loop is observed at $d = 0.8$ nm and $\rho \approx 0.85$–1.1 g/cm³, corresponding to a first order transition between a BL and a THL. No signature of a loop occurs for approximately $d > 0.9$ nm and $d < 0.7$ nm. At $d = 0.6$ nm, the THF at high density transforms into a BI. The perfect BI ($d = 0.6$ nm) occurs at $\rho = 0.93$ g/cm³ [arrow in (b)] and sublimes at lower densities. The BL transforms into a vapor phase at $\rho < 0.7$ g/cm³, for $d \geq 0.7$ nm, and $\rho < 0.87$ g/cm³, for $d = 0.65$ nm.

average density in a slab of width 0.0411 nm located at z. At low density ($\rho = 0.8$ g/cm³) we find a BL, as indicated by the two wide peaks of $\rho(z)$. At high density ($\rho = 1.15$, 1.05 g/cm³), the system is characterized by three layers corresponding to the three peaks in $\rho(z)$. $\rho(z)$ is qualitatively unchanged when going from $\rho = 1.15$ to 1.05 g/cm³. In contrast, when going from $\rho = 1.05$ to 0.95 g/cm³, a dramatic change in structure begins to occur. At $\rho = 0.95$ g/cm³, in the coexistence region, $\rho(z)$ shows three distinct, but not sharp, peaks. The central layer at $z = 0$, rapidly disappears as the density decreases further, down to $\rho = 0.8$ g/cm³. Figure 2(c) shows $\rho(z)$ at $\rho = 0.95$ g/cm³ and the density profile obtained from a linear combination of the profiles at $\rho = 0.9$ g/cm³ and $\rho = 1.05$ g/cm³, which correspond to the low- and high-density stable phases. The overlapping of the profiles in Fig. 2(c) supports the view that, in the coexistence region, the systems is a mixture of two phases. This view is further supported by instantaneous configurations (see below).
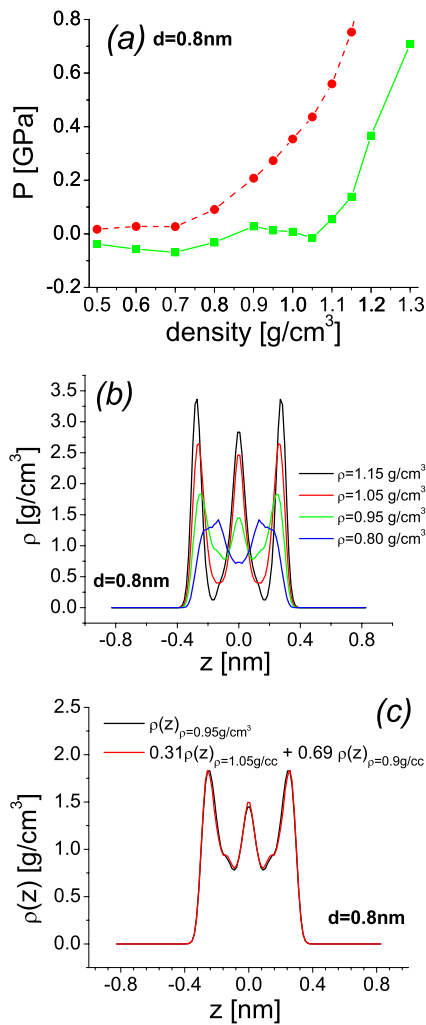
FIG. 2 (color online). (a) Perpendicular ($P_\perp$, dashed line) and parallel ($P_\parallel$, solid line) pressure at $d = 0.8$ nm. The finite size loop characterizing a first order transition is observable only in $P_\parallel(\rho)$. (b) Density profile, $\rho(z)$, for densities above ($\rho = 1.15$, 1.05 g/cm^3) and below ($\rho = 0.8$ g/cm^3) the phase transition indicated in (a), and in the coexistence region ($\rho = 0.95$ g/cm^3). As density decreases from $\rho = 1.15$ g/cm^3 down to $\rho = 0.8$ g/cm^3, water structure changes from trilayer to bilayer. (c) Comparison of the density profile at $\rho = 0.95$ g/cm^3 and that obtained from a linear combination of the density profiles corresponding to the bilayer and trilayer phases ($\rho = 0.9$ g/cm^3 and $\rho = 1.05$ g/cm^3). The overlapping of both density profiles in (c) suggests that at $\rho = 0.95$ g/cm^3 the system is a mixture of the two phases.

The nature of the trilayer system is readily established by visualizing structures. Figures 3(a) and 3(b) show typical water molecule arrangements in the THF, at $\rho = 1.15$ g/cm^3. We divide the confined space into three slabs: the slabs next to the left and right walls ($z < -0.18$ nm and $z > 0.18$ nm, respectively), and the central slab (-0.18 nm $< z < 0.18$ nm). These definitions are based on the location of the minima in $\rho(z)$ observed at $\rho = 1.15$ g/cm^3 [Fig. 2(b)]; such minima are at $z =$
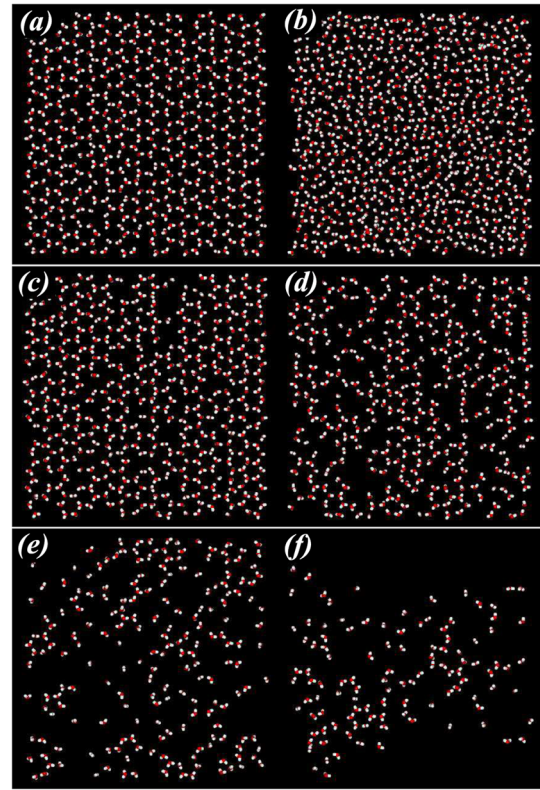
FIG. 3 (color online). (a),(b) Snapshot of the system at $\rho = 1.15$ g/cm^3, $d = 0.8$ nm, and $t = 500$ ps. Molecules are located in (a) a slab of width 0.22 nm next to one of the walls (-0.40 nm $< z < -0.18$ nm), and (b) at the central slab (-0.18 nm $< z < 0.18$ nm). (c)–(f) Same as (a) for water molecules at $\rho = 1.05$, 0.95, 0.8 and 0.5 g/cm^3, respectively. At $\rho = 1.15$ g/cm^3, water molecules next to the walls arrange in an ordered (crystal-like) structure as observed in the BI found at $d = 0.6$ nm (see also Ref. [24]). As density decreases, an order-disorder structural change occurs in the slab next to the walls. No order is observed beyond this slab at any density.

± 0.18 nm. Figures 3(a) and 3(b) show the water molecules in the slab next to one of the walls and in the central slab, respectively. The central slab is liquidlike; it shows no long range order and molecules are readily able to diffuse. Instead, molecules next to the walls arrange in a crystal-like structure and do not diffuse. In fact, water molecule oxygens next to the walls arrange in the same lattice as that corresponding to the BI (see Ref. [24]). The water molecule hexagons observed in Fig. 3(a) are centered at the SiO$_4$ tetrahedra of the wall that protrude into the confined liquid [24]. The crystal-like structure of this slab is, therefore, *templated* by the wall.

Figures 3(c)–3(e) show the typical arrangements of water molecules in a slab next to the walls, at $\rho = 1.05$, 0.95 and 0.8 g/cm^3, respectively [same densities shown in Fig. 2(b)]. At $\rho = 1.05$ g/cm^3, the water structure is still crystal-like and resembles that of Fig. 3(a). Only a few isolated defects, primarily vacancies, are observed. These are transient and appear and disappear randomly across the slab. As density decreases, the size of these gaps increases,

and the water structure is more disordered. At $\rho = 0.95$ g/cm^3, in the coexistence region, water structure shows random hexagons that are barely visible in Fig. 3(d). At $\rho = 0.8$ g/cm^3, where the BL is stable, no order is observed [see Fig. 3(e)]. Comparing the evolution of water at the interface, from Fig. 3(c) to Fig. 3(e), it seems that the THF-to-BL transition is associated with an order-to-disorder transformation or ''melting'' of the interfacial slab. We note that no cavitation occurs in Fig. 3(e). Such a cavitation is observed at $\rho = 0.5$ g/cm^3 [Fig. 3(f)]. The empty regions in Fig. 3(f) expand across the whole confined space. We note that no structural order has been observed in the central slab at any density.

In summary, we have presented results from molecular dynamics simulations of water under nanoconfinement using hydrophobic structured walls. We observed that for a wall-wall separation of $d = 0.8$ nm, where three water layers can fit, a first order transition occurs with increasing density between a BL and a THF. This transition is templated by the walls and manifests water structures distinct from those characteristic of the bulk. The transition is identified as a disorder-order transformation or ''freezing'' of water in the slab next to the walls, as density increases. The first order transition disappears as d increases or decreases from $d = 0.8$ nm. It is thus possible, that the corresponding first order transition line (in the $P_\parallel - d$ plane) is born and ends in two critical points located at large and small d, respectively. At $d = 0.6$ nm, the THF transforms into a BI as density decreases. The kind of surface-templated phase transitions observed here might be a general phenomenon common to other confined liquids. Our results, based on a simplified water and surface model, strongly indicate a different behavior of nanoscale confined systems from that in the bulk.

[1] Y.-K. Cheng and P. J. Rossky, Nature (London) **392**, 696 (1998).
[2] J. Roziere and D. J. Jones, Annu. Rev. Mater. Res. **33**, 503 (2003).
[3] B. Bushan, J. N. Israelachvili, and U. Landman, Nature (London) **374**, 607 (1995).
[4] A. Darhuber and S. M. Troian, Annu. Rev. Fluid Mech. **37**, 425 (2005).
[5] V. F. Petrenko and R. W. Whitworth, *Physics of Ice* (Oxford University Press, New York, 1999).
[6] P. G. Debenedetti, J. Phys. Condens. Matter **15**, R1669 (2003).
[7] J. C. Liu and P. A. Monson, Langmuir **21**, 10 219 (2005); Ind. Eng. Chem. Res. **45**, 5649 (2006).
[8] A. Striolo, A. A. Chialvo, P. T. Cummings, and K. E. Gubbins, Langmuir **19**, 8583 (2003).
[9] A. Striolo, K. E. Gubbins, A. A. Chialvo, and P. T. Cummings, Mol. Phys. **102**, 243 (2004).
[10] A. Striolo, A. A. Chialvo, P. T. Cummings, and K. E. Gubbins, J. Chem. Phys. **124**, 074710 (2006).
[11] K. Koga, X. C. Zeng, and H. Tanaka, Phys. Rev. Lett. **79**, 5262 (1997); Chem. Phys. Lett. **285**, 278 (1998); Nature (London) **408**, 564 (2000).
[12] J. Slovák, K. Koga, H. Tanaka, and X. C. Zeng, Phys. Rev. E **60**, 5833 (1999).
[13] K. Koga, J. Chem. Phys. **116**, 10 882 (2002).
[14] K. Koga and H. Tanaka, J. Chem. Phys. **122**, 104711 (2005).
[15] I. Brovchenko, A. Geiger, A. Oleinikova, and D. Paschek, Eur. Phys. J. E **12**, 69 (2003).
[16] I. Brovchenko, A. Geiger, and A. Oleinikova, J. Chem. Phys. **120**, 1958 (2004); J. Phys. Condens. Matter **16**, S5345 (2004).
[17] I. Brovchenko and A. Oleinikova, J. Chem. Phys. **126**, 214701 (2007).
[18] M. Meyer and H. E. Stanley, J. Phys. Chem. B **103**, 9728 (1999).
[19] P. Kumar, S. V. Buldyrev, F. W. Starr, N. Giovambattista, and H. E. Stanley, Phys. Rev. E **72**, 051503 (2005).
[20] P. Kumar, F. W. Starr, S. V. Buldyrev, and H. E. Stanley, Phys. Rev. E **75**, 011202 (2007).
[21] K. Koga, G. T. Gao, H. Tanaka, and X. C. Zeng, Nature (London) **412**, 802 (2001).
[22] J. Bai, J. Wang, and X. C. Zeng, Proc. Natl. Acad. Sci. U.S.A. **103**, 19 664 (2006).
[23] R. Zangi and A. E. Mark, Phys. Rev. Lett. **91**, 025502 (2003); J. Chem. Phys. **119**, 1694 (2003).
[24] N. Giovambattista, P. J. Rossky, and P. G. Debenedetti, Phys. Rev. E **73**, 041604 (2006).
[25] N. Giovambattista, P. G. Debenedetti, and P. J. Rossky, J. Phys. Chem. C **111**, 1323 (2007); J. Phys. Chem. B **111**, 9581 (2007).
[26] R. K. Iler, *The Chemistry of Silica* (Wiley, New York, 1979); C. Hammond, *The Basics of Crystallography and Diffraction* (Oxford University Press, New York, 2001).
[27] H. J. C. Berendsen, J. R. Grigera and T. P. Stroatsma, J. Phys. Chem. **91**, 6269 (1987).
[28] A. Y. Toukmaji and J. A. Board Jr., Comput. Phys. Commun. **95**, 73 (1996).
[29] T. M. Nymand and P. Linse, J. Chem. Phys. **112**, 6152 (2000).
[30] *Reviews in Computational Chemistry*, edited by S. Klapp and M. Schoen (John Wiley & Sons, Hoboken, 2007). Vol. 24;
[31] T. M. Truskett, P. G. Debenedetti, and S. Torquato, J. Chem. Phys. **114**, 2401 (2001).
[32] L. G. MacDowell, P. Virnau, M. Müller, and K. Binder, J. Chem. Phys. **120**, 5293 (2004); K. Binder, Eur. Phys. J. B **64**, 307 (2008).
[33] K. B. Jinesh and J. W. M. Frenken, Phys. Rev. Lett. **101**, 036101 (2008).